ACS APPLIED MATERIALS & INTERFACES

Research Article

www.acsami.org

Facile Conversion of Commercial Coarse-Type $LiCoO_2$ to Nanocomposite-Separated Nanolayer Architectures as a Way for Electrode Performance Enhancement

Yinan Zhao,[†] Yujing Sha,[†] Qian Lin,[†] Yijun Zhong,[†] Moses O Tade,[‡] and Zongping Shao*[,†,‡]

[†]State Key Laboratory of Materials-Oriented Chemical Engineering, College of Chemistry & Chemical Engineering, Nanjing Tech University, Nanjing 210009, China

[‡]Department of Chemical Engineering, Curtin University, Perth, Western Australia 6845, Australia

ABSTRACT: Coarse-type $LiCoO_2$ is the state-of-the-art cathode material in small-scale lithium-ion batteries (LIBs); however, poor rate performance and cycling stability limit its large-scale applications. Here we report the modification of coarse-type $LiCoO_2$ (LCO) with nanosized lithium lanthanum titanate ($Li_{3x}La_{2/3-x}TiO_3$, LLTO) through a facile sol−gel process, the electrochemical performance of commercial $LiCoO_2$ is improved effectively, in particular at high rates. The crystalline structure of pristine $LiCoO_2$ is not affected by the introduction of the LLTO phase, while nanosized LLTO particles are likely incorporated into the space of the $LiCoO_2$ layers to form a LCO-LLTO nanocomposite, which separate the LCO layers with the increase of layer spacing to ∼100 nm. The LLTO incorporation through the facile post-treatment effectively reduces the charge-transfer resistance and increases the electrode reactions; consequently, the LLTO-incorporated LCO electrode shows higher capacity than $LiCoO_2$ at a higher rate and prolonging cycling stability in both potential ranges of 2.7−4.2 V and 2.7−4.5 V, making it also suitable for high-rate operation. This novel concept is general, which may also be applicable to other electrode materials. It thus introduces a new way for the development of high rate-performance electrodes for LIBs for large scale applications such as electric vehicles and electrochemical energy storage for smart grids.

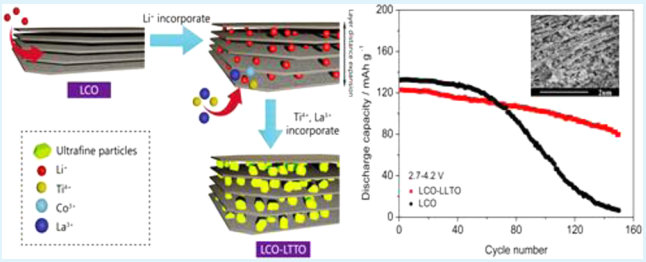

KEYWORDS: *lithium-ion battery, lithium cobalt oxide, solid electrolyte, lithium lanthanum titanate, surface modification*

1. INTRODUCTION

Lithium-ion batteries (LIBs), which show advantageous features of high voltage, no memory effect, environmental benignity, and high energy density, are currently widely used as power sources for personal electronics and many portable devices. Very recently, their large-scale applications in the fields of electric vehicles and smart grids are also well recognized, in which high power/energy density and high safety are required.[1]

$LiCoO_2$, a layered oxide with a distorted α-$NaFeO_2$-type rock-salt structure, in which Li^+ and Co^{3+} distribute alternatively on the (111) planes separated by close-packed oxygen layers,[2] is still the most used cathode material in commercial LIBs for applications as power sources of personal electronics. The lithium in the layer-structured $LiCoO_2$ can be extracted electrochemically at a potential higher than 4.0 V, and typically about half of the lithium can be extracted at a voltage of 4.2 V (vs Li^+/Li), resulting in a reversible capacity of slightly lower than 140 mA h g^{-1}.[3,4] During the delithiation process, the c-axis of the Li_xCoO_2 lattice expands, up to approximately 2.6% at x = 0.5 (∼4.2 vs Li^+/Li).[5] Actually, the lithium can be further extracted at higher potentials; however, phase transition from monoclinic to hexagonal at ∼4.5 V is associated, inducing ∼3% in lattice contraction.[6] Such structural distortion could result in fast capacity decay with the electrochemical cycling. Thus, special care should be taken to avoid overcharge of the electrode. In addition, at higher potentials, the side reactions between pristine $LiCoO_2$ and liquid electrolyte also become a big concern.[7,8] Dissolution of Co^{4+} into a liquid electrolyte is another origin for the degradation in capacity of $LiCoO_2$ electrode during galvanostatic charge−discharge cycling, in particular, at potentials above 4.4 V.[9] On the other hand, conventional commercial $LiCoO_2$ is in coarse type, which shows poor rate capability.[10] Thus, the use of conventional $LiCoO_2$ in large-scale LIBs faces big challenges.

Recently, many strategies have been taken to increase the safety, rate capability, and cycling stability of the $LiCoO_2$ electrode through suppressing structural changes caused by its phase transition and side reactions with electrolyte, and decreasing cobalt dissolution to liquid electrolyte.[11−20] For example, surface coating was widely used to reduce the dissolution of Co^{4+} into a liquid electrolyte by avoiding the direct contact of $LiCoO_2$ with the liquid electrolyte.[11−15] To increase the rate capability, nanosizing the electrode materials through advanced synthesis has been widely tried.[16−20] A

Received: October 25, 2014
Accepted: January 5, 2015
Published: January 5, 2015

DOI: 10.1021/am507421y
ACS Appl. Mater. Interfaces 2015, 7, 1787−1794

dilemma is that nanosizing leads to an increase in specific surface area of the electrode, which may accelerate the dissolution of Co^{4+} into a liquid electrolyte, thus introducing detrimental effect on the cycling stability of $LiCoO_2$. Simultaneous nanosizing and surface coating/structural modification may realize high cycling stability and rate capability simultaneously.[21−26] However, complex synthesis process is usually involved, which largely reduces the practical applicability due to ineffectiveness in commercial competitiveness. In addition, nanosized materials usually show low tap density,[27] which will not only result in low volumetric energy density, but also increase the amount of liquid electrolyte, both are unfavorable for practical LIBs.

The formation of solid lithium electrolyte and electrode material composite was sometimes used in solid-state LIBs to improve the performance by reducing the charge-transfer polarization resistance.[28−30] Previously, we proposed a new concept for improving the rate capability and cycling stability of $Li_4Ti_5O_{12}$ anode by forming micrometer-sized solid lithium electrolyte−$Li_4Ti_5O_{12}$ nanocomposite.[31] The in situ formed $Li_{3x}La_{2/3-x}TiO_3$ (LLTO) solid lithium electrolyte could improve the apparent lithium conductivity of the electrode material, thus effectively reducing the polarization resistance at fast rate, consequently improving the rate performance, while the formation of the composite could reduce the contact surface area between the $Li_4Ti_5O_{12}$ electrode and liquid electrolyte, thus improving the cycling stability.

In this study, we reported a novel way for the facile conversion of commercial coarse-type $LiCoO_2$ to a solid lithium electrolyte−$LiCoO_2$ nanocomposite with a unique morphological structure and low specific surface area through a facile chemical process. As mentioned previously, coarse-type $LiCoO_2$ is still the most applied cathode material in commercial LIBs, which is typically prepared by a solid-state reaction. Currently, the mass production of $LiCoO_2$ is highly matured with low cost; however, the coarse-type particle size limits its high rate performance. Through convenient treatment of commercial pristine $LiCoO_2$ oxide, the as-obtained product showed much improved cycling stability and rate capability. Although LLTO has negligible capacity at the cathode potential, however, a small amount (5 wt %) of LLTO incorporation had no obvious effect on the theoretical capacity. It thus provides a unique technique that may greatly extend the application of commercial $LiCoO_2$ potentially also into the field of electric vehicles.

2. EXPERIMENTAL SECTION

2.1. Materials Synthesis. The modification of commercial HT-$LiCoO_2$ (99.8%, Aladdin) with lithium lanthanum titanate, $Li_{3x}La_{2/3-x}TiO_3$ ($3x$ = 0.35) was conducted through a combined EDTA-CA complexing sol−gel method. During the modification, analytical reagents of lithium nitrate ($LiNO_3$) (AR), lanthanum(III) nitrate hydrate ($La(NO_3)_3{\cdot}6H_2O$) (AR), and tetrabutyl titanate ($Ti(OC_4H_9)_4$) (CP) were used as starting materials to prepare LLTO sols.[32] The as-obtained sols were diluted with a certain amount of distilled water and then mixed with commercial $LiCoO_2$ coarse particles. After the solution was stirred at 80 °C for 2 h, the $LiCoO_2$-LLTO sols mixture was heated at 250 °C in an electric oven for 12 h to obtain a solid precursor, which was then conducted further heat treatment in air at 500−700 °C for 8 h to result the desired composite. The relatively low heat treatment temperatures were selected to suppress the formation of secondary phases through potential reactions between $LiCoO_2$ and LLTO phases.

2.2. Material Characterization. The crystal structures of commercial LCO and the as-prepared LCO-LLTO composites were characterized by room-temperature X-ray diffraction patterns (XRD, Rigaku Smartlab diffractometer). Cu Kα radiation was used as an X-ray source. The particulate morphologies and particle size distributions of the materials were observed using scanning electron microscopy (FESEM, HITACHI S-4800) and transmission electronic microscopy (TEM, FEI Tecnai G2T20), and high-resolution transmission electron microscopy (HRTEM, FEI Tecnai G2T20) with an accelerating voltage of 200 kV. The specific surface area of the samples was obtained by N_2 adsorption at the temperature of liquid nitrogen by the BEL SORP II instrument after being pretreated at 250 °C.

2.3. Electrochemical Test. The electrochemical performances of pristine LCO and LCO-LLTO composite oxides were carried out with CR2016-type coin cells using metallic lithium film as the counter and reference electrodes, and with a liquid electrolyte of 1 M $LiPF_6$ in a 1:1 (v/v) ethylene carbonate and dimethyl carbonate mixture. Microporous polypropylene (PP) membrane (Celgard, 2400) was used as the separator. The traditionally fabricated $LiCoO_2$ porous composite electrode was prepared by spreading a mixture of $LiCoO_2$ powder, conductive Super P (NCM HERSBIT Chemical Co., Ltd., China), PVDF (polyvinylidene fluoride, Aldrich) (85:8:7 in weight) with *N*-methyl-2-pyrrolidone on a piece of Al foil. The slurry-covered Al foil was dried in a vacuum at 100 °C for 12 h before electrochemical evaluation. Cell assembly was conducted in a glovebox filled with pure argon atmosphere.

The electrochemical performances of the as-prepared electrode materials were tested using a NEWARRE BTS 5 V-50 mA computer-controlled battery test station (Shenzhen, China) at room temperature (~25 °C). The tests were performed under two potential ranges of 2.7−4.2 V and 2.7−4.5 V. Cyclic voltammetry tests were performed over two potential ranges using a Princeton Applied Research potentiostat/galvanostat model 273A at the scanning rate of 0.1 mV s^{-1}. Complex impedance measurements were also carried out with Princeton 2273 electrochemical workstation over the single cell at the state of discharging. A perturbation of 10 mV was applied and data collected under PC control and the frequency range applied is from 100 kHz to 100 mHz.

3. RESULTS AND DISCUSSION

3.1. Structural and Morphological Properties. Shown in Figure 1 are the room-temperature XRD patterns of commercial pristine $LiCoO_2$ powder and the various LLTO-incorporated $LiCoO_2$ composites prepared from the facile treatment of commercial coarse-type $LiCoO_2$ with LLTO precursor in combination with a subsequent cocalcination in air at different temperatures for 5 h. The XRD patterns of the pristine $LiCoO_2$ can be well indexed based on the α-$NiFeO_2$ structure, where alternating planes containing Li and Co ions are separated by close-packed oxygen layers. The obtained diffraction profiles were analyzed by the Rietveld method with the GSAS-EXPGUI package.[33] Rietlveld refinement of the XRD patterns based on the stoichiometric rhombohedral structure of the $R\bar{3}m$ space group gives lattice constants a/b and c, respectively, of 2.8173(2) Å and 14.057(0) Å (c/a = 4.987) with low error (LCO R_p = 2.91%, R_{wp} = 7.30%, χ^2 = 3.746, α = β = 90°, γ = 120°, $R\bar{3}m$), which agree well with the literature results.[34]

After the LLTO phase was introduced, the LCO phase was always presented irrespect of the calcination temperatures, although its peak intensity was reduced somewhat, suggesting the phase reaction between LCO and LLTO precursor was not very serious at a calcination temperature lower than 700 °C. As for LLTO itself, its crystalline phase appeared in the samples when the calcination was conducted at 600 or 700 °C. The XRD patterns of the LCO-LLTO composites calcined at 600 or

DOI: 10.1021/am507421y
ACS Appl. Mater. Interfaces 2015, 7, 1787−1794

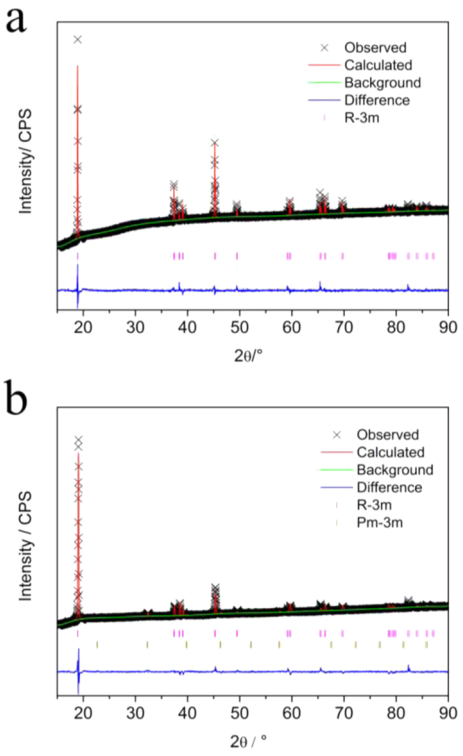

Figure 1. XRD patterns of (a) $LiCoO_2$ and (b) LCO-LLTO composite.

700 °C were then subjected for Rietlveld refinement based on a physical mixture of LCO and LLTO. Good fitting with low error was obtained, which further suggests the negligible reaction between the LCO and LLTO phases. For example, for the LCO-LLTO composite calcined at 700 °C, the XRD patterns were well refined based on a mixture of LCO ($a = b = 2.817(9)$ Å, $c = 14.05(8)$ Å, $\alpha = \beta = 90°$, $\gamma = 120°$, $R\bar{3}m$, 95.1 wt %) and LLTO ($a = b = c = 3.92(3)$ Å, $\alpha = \beta = \gamma = 90°$, $Pm\bar{3}m$, 4.9 wt %) with low error ($R_p = 5.59\%$, $R_{wp} = 9.89\%$, $\chi^2 = 7.431$). The c/a value of the LCO phase was found to be 4.987, 4.987, and 4.986 for the LCO phase in pristine LCO and LCO-LLTO composites calcined at 600 or 700 °C, respectively. The results suggest no obvious incorporation of Ti and La from LLTO into LCO happened during the calcination at either 600 or 700 °C.

To demonstrate the effect of LLTO incorporation on the morphological structure of LCO particles, both the pristine LCO and LLTO-incorporated LCO composite after the calcination at 700 °C were subjected for SEM observation, with the typical images in different magnifications shown in Figure 2. The pristine LCO particles had size of 5−15 μm and were in a semisphere particulate shape with round grain edge and smooth surface (Figure 2a). The smooth surface was more clearly demonstrated in images with larger magnifications, as shown in Figure 2b,c. By a careful observation of the SEM image in Figure 2d, it was found that the LCO particles were actually in rock-like layered structures, although the individual layers were closely packed. As for the LCO-LLTO composite calcined at 700 °C, although the main particle size did not change obviously as compared to the pristine LCO, the surface of the secondary particles in LCO-LLTO became much rougher (Figure 2a′). It looks that the LCO particles were corroded after the calcination together with the LLTO precursor. In addition, the edge of the particles became sharper after the reaction. From the SEM images with larger

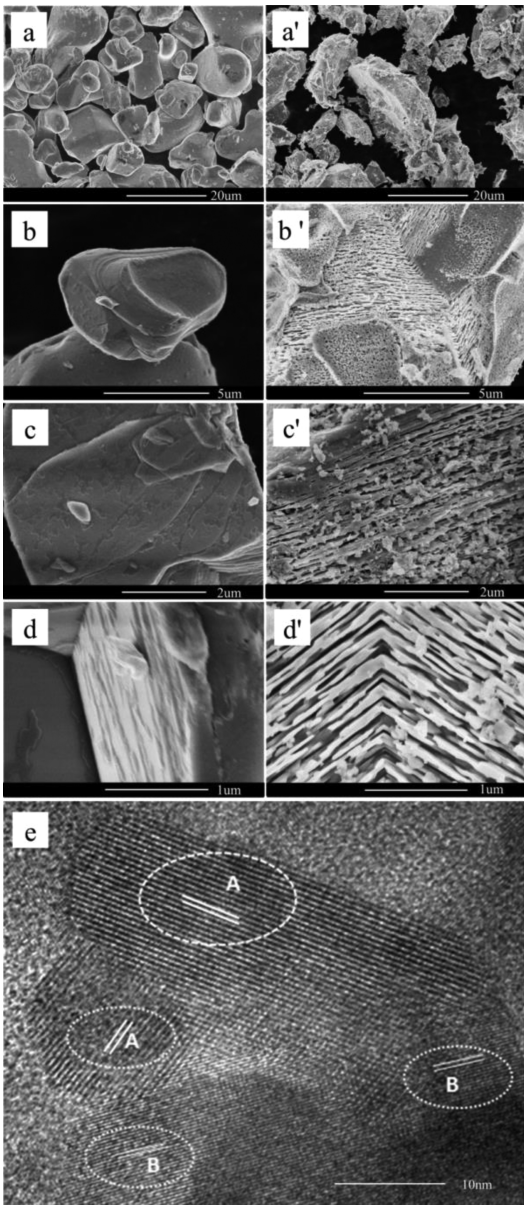

Figure 2. SEM images of (a, b, c, d) LCO and (a′, b′, c′, d′) LCO-LLTO, and (e) HR-TEM image of the ultrafine particles as shown in panel c′.

magnification (Figure 2b′−d′), many ultrafine particles with the size of hundreds of nanometers were clearly observed over the surface of primary particles, which demonstrated clear layer-structured morphological shape with much enlarged layer spacing than the pristine $LiCoO_2$. As shown in Figure 2c′,d′, the layers have the thickness of 100−200 nm, which were separated by ultrafine particles with the size of around 100 nm, creating the layer spacing of around 100 nm.

To get further information about the composition of the ultrafine particles in the LCO-LLTO composite, they were subjected for energy-dispersive X-ray spectroscopy (EDX) analysis. The surface of the secondary particles showed an average Ti to Co atomic ratio of 1:46, which is very close to the average molar ratio of Ti to Co in the whole composite (1:40). It was found that the layer was mainly composed of Co and O elements, although signals of La and Ti in low intensity were also detected. For example, the atomic ratio of Ti to Co is

DOI: 10.1021/am507421y
ACS Appl. Mater. Interfaces 2015, 7, 1787−1794

1:220, which is much lower than the average Ti to Co ratio in the LCO-LLTO composite (1:40). It suggests the layers were likely composed of the LCO phase. It should be mentioned that because of the lightweight of Li, it is insensitive by EDX and thus not detectable. Due to resolution limitation, the current SEM-EDX could not detect the composition of particles with size smaller than 100 nm, thus the composition of the ultrafine particles were subjected for HR-TEM and STEM analysis. Shown in Figure 2e is the typical HR-TEM image of the ultrafine particles; diffraction fringes with different distances of 0.465 nm (mark A) and 0.274 nm (mark B) were demonstrated, which can be well indexed based on the diffraction plane (003) for LCO and (110) diffraction plane for spinel LLTO. It suggests such ultrafine particles were actually composed of LCO and LLTO phases.

To get further information about the composition of the ultrafine particles, STEM analysis was also conducted. As shown in Figure 3a is TEM image of a grain with the size of 250

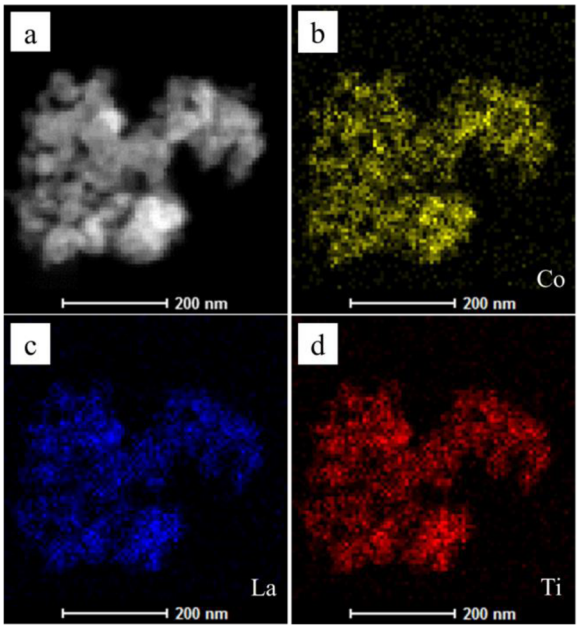

Figure 3. (a) TEM image for the ultrafine particles and the related EDX mapping images of (b) Co, (c) La, and (d) Ti.

nm which was subjected for EDX mapping of Co, La and Ti elements. It was found that the Co, La, and Ti distributed homogeneously all over the grain (Figure 3b–d), suggesting the highly uniform distribution of the two phases (LCO and LLTO) inside the ultrafine particles. The atomic ratio of Ti to Co was found to be around 1:1, which is much larger than the average ratio in the composite (1:40). It further suggests that the LLTO phase mainly incorporated into the ultrafine particles which separated the layers to create large layer spacing. Based on the above analysis, it is likely that the LLTO phase mainly incorporated into the spaces of LCO layers, which formed a nanocomposite with the LCO phase to separate the LCO layers. Such a unique nanocomposite-separated nanolayers morphological structure can facilitate the electrode reaction, and the penetration of liquid electrolyte, thus benefiting the lithium intercalation reactions.

Shown in Figure 4 is the nitrogen adsorption/desorption curve of the LCO-LLTO composite. Interestingly, it demonstrated a type II according to IUQAC definition, suggestion the

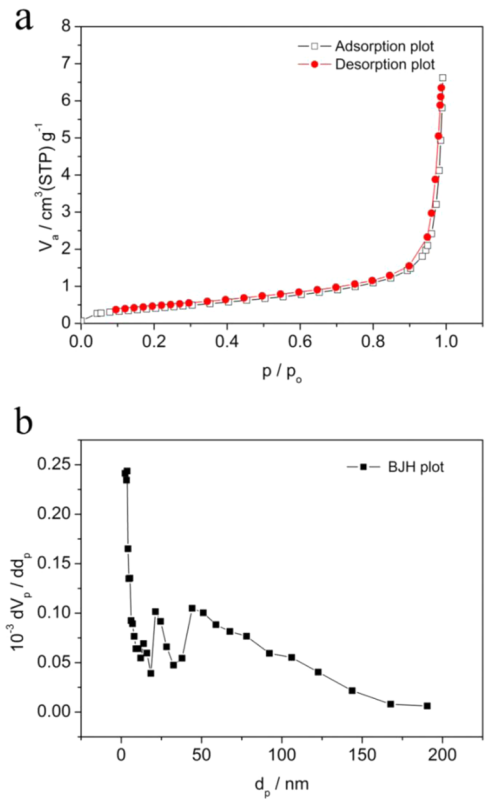

Figure 4. (a) Nitrogen adsorption–desorption isotherms and (b) pore size distribution curve of the LCO-LLTO composite.

lack of mesopores. The specific surface area according to BET method is 1.59 m^2 g^{-1}, which is only slightly larger than that of the pristine LCO (0.36 m^2 g^{-1}), still sufficiently low to minimize contacting area between the electrode and the liquid electrolyte. As we know, the cobalt dissolution is closely related to the electrode surface area. The low specific surface area further confirmed the lack of micro and mesopores in the LCO-LLTO composite, those pores usually contribute significantly to the specific surface area of a material. From the BJH pore size distribution, as shown in Figure 4b, a non-negligible fraction of pores below 50 nm (mesopores) was also observed. It suggests that the incorporation of LLTO into the LCO phase could not only expand the layer space of LCO phase, it likely also created some defects over the LCO layers, thus introducing additional mesopores.

On the basis of the above analysis, a mechanism for the formation of the special morphological shape of the LCO-LLTO nanocomposite by the facile post treatment of commercial coarse-type $LiCoO_2$ was proposed, and is schematically shown in Figure 5. The pristine $LiCoO_2$ was in a layer structure; however, the layers were closely packed to form a coarse-type particulate morphology. By calcining coarse LCO together with LLTO gel precursor, the Li cations from LLTO precursor were likely incorporated into the space of the LCO layers through possible surface defects by chemical diffusion under thermally activation because of its small cation size. The incorporation of lithium led to expansion of the layer distance. Then La and Ti cations were also able to diffuse into the layer spaces, which reacted with the Li that was diffused from LLTO precursor with the formation of LLTO, consequently LCO-LLTO nanocomposites were formed between the layers of LCO. Such nanocomposite grew to the

DOI: 10.1021/am507421y
ACS Appl. Mater. Interfaces 2015, 7, 1787–1794

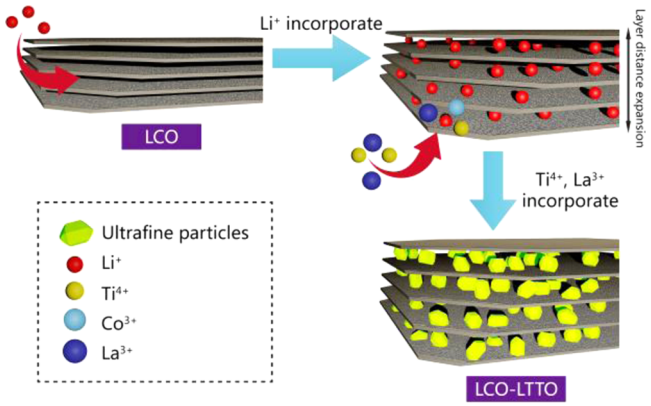

Figure 5. Proposed mechanism for the formation of the special morphology of the LCO-LLTO nanocomposite.

size of around 100 nm, likely controlled by the amount of LLTO in the starting precursor (~5 wt %). The growth of LCO-LLTO nanocomposites then expanded the layer distance of the LCO to the size of the nanocomposites (around 100 nm), allowing the easy penetration of liquid electrolyte, which should be beneficial for electrochemical reaction.

3.2. Electrochemical Performance. To exploit the effect of the incorporation of LLTO phase on the electrochemical performance of the LCO electrode, the LCO-LLTO composite from the calcination at 700 °C was used as a working electrode of a half cell and subjected for the electrochemical test for lithium intercalation/deintercalation reactions; for comparison, the commercial pristine LCO was also evaluated. Shown in Figure 6 are the first charge−discharge curves for both the pristine LCO and the LCO-LLTO composites (calcined at 700 °C) at a current rate of 0.2 C, and two potential ranges of 2.7−4.2 V and 2.7−4.5 V were tried. At a potential window of 2.7−4.2 V, a first discharge capacity of 132 mAh g^{-1} was achieved for the LCO electrode, while it was around 121 mAh g^{-1} for the LCO-LLTO composite electrode. By considering the negligible capacity of LLTO at the high potential range (2.7−4.2 V), the slightly lower capacity of the LCO-LLTO composite than that of LCO is well understood. The overlapping for most parts of the charge−discharge curves for the two electrodes suggests that the phase structure of LCO in LCO-LLTO was not significantly altered, agreeing well with the XRD and TEM results. The lower than 140 mAh g^{-1} capacities for both electrodes are in good agreement with the fact that usually less than 0.5 Li in LCO can be reversibly extracted at a voltage lower than 4.2 V. By increasing the up-terminal potential to 4.5 V, the capacities increased as expected, reaching 183 mAh g^{-1} for the LCO electrode and 154 mAh g^{-1} for the LCO-LLTO composite electrode. It suggests more lithium was extracted from the Li_xCoO_2 lattice at higher potentials.

The discharge capacities for the LCO and the LCO-LLTO electrodes at different rates were further tested at both selected potential ranges (2.7−4.2 V and 2.7−4.5 V), and the results are shown in Figure 7. Although at lower discharge rates, the LCO electrode had a higher capacity than the LCO-LLTO composite electrode (Figure 7a), its capacity decreased faster at a higher rate. At a discharge rate of 5.0 C, the LCO-LLTO electrode started to show a higher capacity than the LCO electrode, i.e., 80 and 70 mAh g^{-1} for the LCO-LLTO and the LCO electrodes, respectively. The capacity retention percentages at different current rates, compared to that at 0.2 C rate, are also

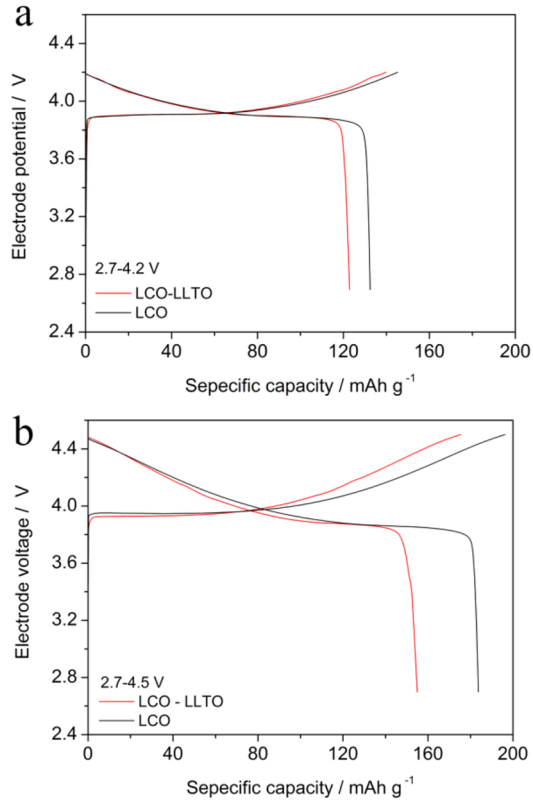

Figure 6. Initial charge and discharge curves for LCO and LCO-LLTO composite at a current rate of 0.2 C in different potential ranges: (a) 2.7−4.2 V and (b) 2.7−4.5 V.

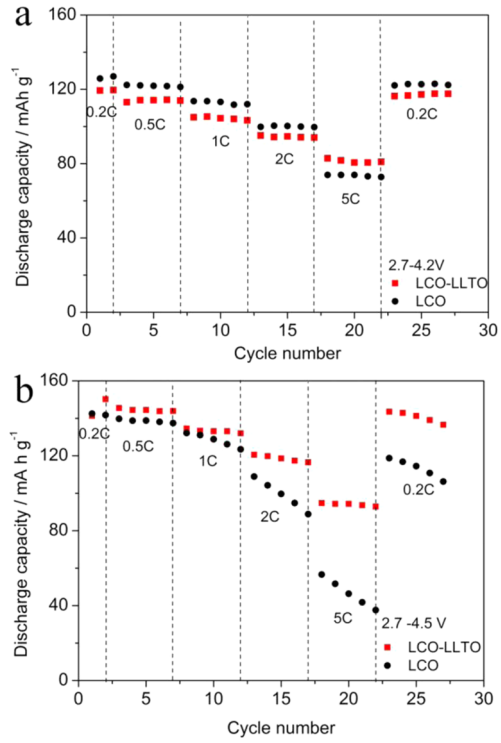

Figure 7. Rate performance of the LCO and LCO-LLTO composite electrodes at different current rates at two different potential ranges: (a) 2.7−4.2 V and (b) 2.7−4.5 V.

presented in Figure 7a. It indicates that the LCO-LLTO electrode always had higher capacity retention than the LCO

DOI: 10.1021/am507421y
ACS Appl. Mater. Interfaces 2015, 7, 1787−1794

electrode, suggesting the effectiveness of incorporation of LLTO solid lithium electrolyte in improving the rate performance of the LCO electrode. At the potential window of 2.7−4.5 V, the better capacity retention at higher rate by incorporating LLTO phase is more eminent, as shown in Figure 7b. At a current rate of 1.0 C, the LCO-LLTO electrode started to show higher absolute capacity than the LCO electrode. Interestingly, the LCO electrode showed a quick decay in capacity with the cycling time at a faster rate, while the LCO-LLTO composite showed much better stability during the cycling. After cycling at various rates for 25 times, the capacity of the LCO-LLTO composite electrode can restore to the original capacity value at 0.2 C when the discharge rate is reset to 0.2 C. However, as for the LCO electrode, after tests at various rates, the capacity was only 120 mAh g^{-1} when the discharge rate was reset to 0.2 C, as compared to 150 mAh g^{-1} for the initial capacity at 0.2 C. The above results strongly suggest the incorporation of the LLTO phase also greatly improved the cycling stability of the LCO electrode.

To explain the improved electrochemical performance of the LCO electrode by incorporating the LLTO phase, the EIS of both the pristine LCO and LCO-LLTO composite (700 °C calcined) electrodes were measured at 2.7 V, and typical results are shown in Figure 8. The EIS of both electrodes showed a semicircle at the high-to-low frequency range and a tail at the low frequency range. The semicircle is generally postulated to be related with the charge-transfer process of the electrode reaction.[35] For the LCO electrode, a polarization resistance of around 250 Ω was demonstrated associated with the charge-transfer process (the semi arc in impedance spectra), while it was only 40 Ω for the LCO-LLTO electrode. The incorporation of LLTO likely increased the apparent lithium-ion conductivity of the electrode on the one hand, whereas the creation of nanocomposite-separated nanolayers particulate morphology allowed the easy penetration of liquid electrolyte on the other hand. Both modifications/improvements could effectively reduce the lithium-ion charge-transfer polarization resistance associated with the electrode reactions, thus helping to the improved rate performance of the LCO electrode.

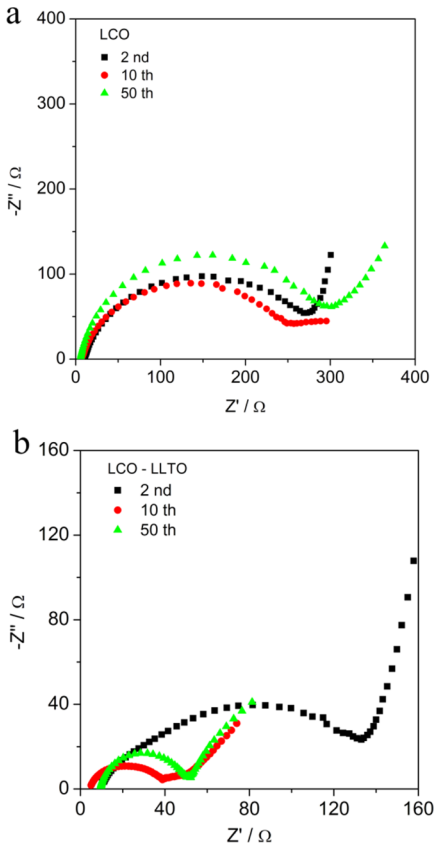

Figure 8. EIS of the (a) LCO and (b) LCO-LLTO composite electrodes after 2, 10, and 50 charge−discharge cycles at a current rate of 0.2 C in the potential ranges of 2.7−4.2 V.

To further demonstrate the beneficial effect of incorporating the LLTO phase into LCO for improving the cycling stability, both electrodes were cycled at a charge−discharge rate of 0.2 C for 150 times, and two potential ranges of 2.7−4.5 V and 2.7−4.2 V were tried. As shown in Figure 9a, at the potential window of 2.7−4.2 V, the LCO and LCO-LLTO electrodes showed similar decay rates in capacity within the first 50 cycles; however, with further cycling, the capacity of the LCO electrode decreased more quickly with the cycling times, and it decreased to less than 10 mAh g^{-1} after 150 galvanostatic charge−discharge cycles. As for the LCO-LLTO composite electrode, a capacity of around 80 mAh g^{-1} was still maintained after the same 150 charge−discharge cycles, indicating a capacity retention of 65%. By cycling at the wider potential window of 2.7−4.5 V, as shown in Figure 9b, the capacity for the LCO electrode decreased almost linearly with cycling time, with a capacity of only 30 mAh g^{-1} after 150 galvanostatic charge−discharge cycles. As for the LCO-LLTO composite electrode, although a fast decay in capacity was also observed at the first 40 cycles, the capacity was stabilized with the further charge−discharge cycling, and a capacity of around 60 mAh g^{-1} was still obtained after 150 cycles, which is about 2 times that of

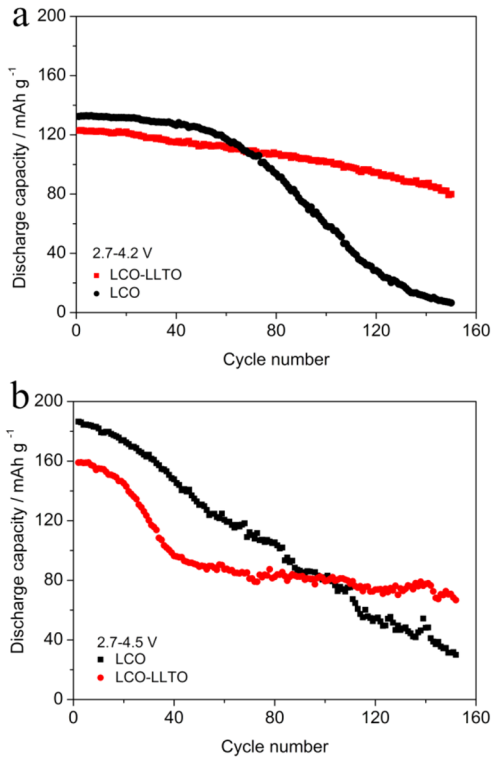

Figure 9. Cycling performance of the LCO and LCO-LLTO composite electrodes at a current rate of 0.2 C in two different potential ranges of (a) 2.7−4.2 V and (b) 2.7−4.5 V.

DOI: 10.1021/am507421y
ACS Appl. Mater. Interfaces 2015, 7, 1787−1794

LCO. The above results clearly demonstrated the superior cycling stability of the LLTO incorporated LCO than the pristine LCO. The better cycling stability of LCO-LLTO than pristine LCO was also demonstrated by the cyclic voltammetry. Shown in Figure 10 are the cyclic voltammetry of LCO and LCO-LLTO electrodes at the first and tenth cycles, cycling with the potential window of 2.7−4.5 V. For the LCO electrode, although the redox peaks are sharp, suggesting the good cycling reversibility, the cyclic voltammetry peaks became much broader after the tenth cycle while the peak current was reduced significantly. It suggests the significant decoration of electrode reaction kinetics with cycling time. As to LCO-LLTO, after tenth cycle, the cyclic voltammetry curves still showed good overlap with the initial cyclic voltammetry curves, indicating the electrode reaction kinetics were well retained.

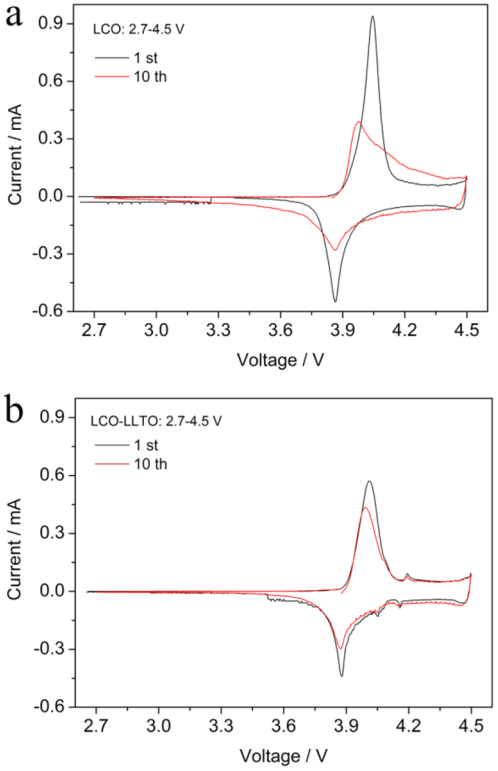

Figure 10. Cyclic voltammograms of (a) LCO and (b) LCO-LLTO electrode at the first and tenth charge−discharge cycles in the potential range of 2.7−4.5 V.

Figure 11 shows the SEM images of LCO and LCO-LLTO electrodes after the cycling at potential window of 2.7−4.2 V for 0.2 C for 80 cycles. It demonstrates that the LCO electrode showed a well sintered morphology structure with a smooth surface and unclear layer structure, while the LCO-LLTO still showed good layer structure. The improved cycling stability could be explained by the unique nanocomposite-separated nanolayer particulate morphology and solid lithium electrolyte-LCO nanocomposite feature of the modified electrode. The successful size reduction of micrometer-sized LCO particles to 100−200 nm-sized thin layers separated by ultrafine LCO-LLTO particles could provide sufficient buffer space to release the internal strain during the charge/discharge process, thus effectively improving the cycling stability.

4. CONCLUSIONS

In summary, we successfully developed commercial coarse-type $LiCoO_2$ into a $Li_{3x}La_{2/3-x}TiO_3$ (LLTO)-LCO composite by simply treating the LCO with LLTO sol precursors and further calcination. The diffusion of LLTO into the layers of LCO successfully expanded the layer spacing, which facilitated the penetration of liquid electrolyte, while the specific surface area was not largely changed, ensuring still low cobalt dissolution. The as-prepared LCO-LLTO composite showed both improved rate performance and cycling stability, in particular at a wider potential window of 2.7−4.5 V. For example, the LCO-LLTO composite electrode showed a high capacity of 90 mAh g^{-1} at the rate of 5 C while the pristine LCO electrode

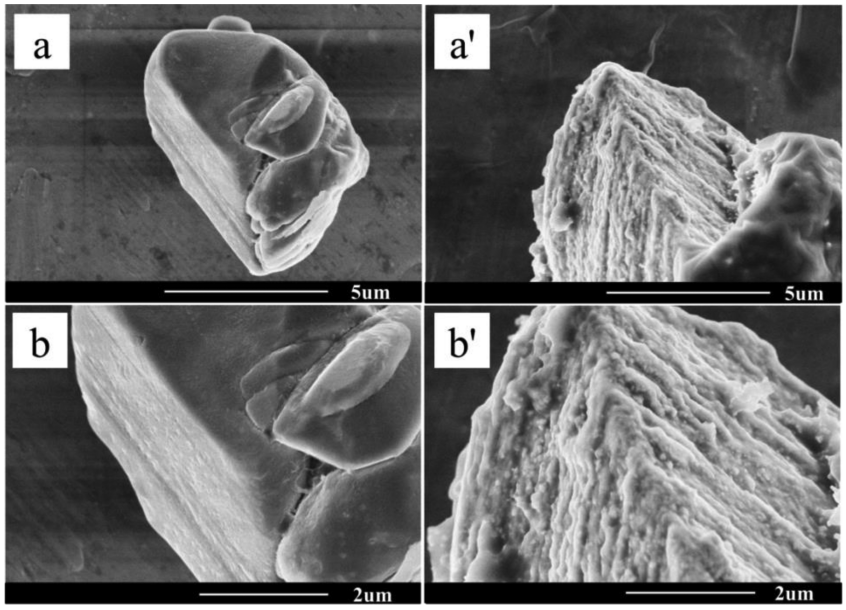

Figure 11. SEM images of (a, b) LCO, and (a′, b′) LCO-LLTO electrode, after charge−discharge cycling at potential window of 2.7−4.2 V for 80 cycles.

DOI: 10.1021/am507421y
ACS Appl. Mater. Interfaces 2015, 7, 1787−1794

showed a capacity of 40 mAh g^{-1} at the potential window 2.7−4.5 V. It thus provides a unique technique that may greatly extend the application of commercial $LiCoO_2$ potentially also into the field of large scale applications, such as electric vehicles.

AUTHOR INFORMATION

Corresponding Author

*Z. Shao. E-mail: shaozp@njtech.edu.cn.

Notes

The authors declare no competing financial interest.

ACKNOWLEDGMENTS

This work was supported by the Key Projects in Nature Science Foundation of Jiangsu Province under contract no. BK2011030, by the National Science Foundation for Distinguished Young Scholars of China under contract no. 51025209, and by the "National Nature Science Foundation of China" under contract no. 21103089. We also thank the Project of Priority Academic Program Development of Jiangsu Higher Education Institutions (PAPD).

REFERENCES

(1) Tarascon, J.-M.; Armand, M. Issues and Challenges Facing Rechargeable Lithium Batteries. *Nature* **2001**, *414*, 359−367.

(2) Fey, G. T. -K.; Kumar, T. P. Long-Cycling Coated $LiCoO_2$ Cathodes for Lithium Batteries — A Review. *J. Ind. Eng. Chem.* **2004**, *10*, 1090−1103.

(3) Chen, Z. H.; Dahn, J. R. Methods to Obtain Excellent Capacity Retention in $LiCoO_2$ Cycled to 4.5 V. *Electrochim. Acta* **2004**, *49*, 1079−1090.

(4) Yang, Z. X.; Yang, W. S.; Evans, D. G.; Li, G.; Zhao, Y. Y. Enhanced Overcharge Behavior and Thermal Stability of Commercial $LiCoO_2$ by Coating with a Novel Material. *Electrochem. Commun.* **2008**, *10*, 1136−1139.

(5) Cho, J.; Kim, Y. J.; Kim, T.-J.; Park, B. Zero-Strain Intercalation Cathode for Rechargeable Li-ion Cell. *Angew. Chem., Int. Ed.* **2001**, *40*, 3367−3369.

(6) Ohzuku, T.; Ueda, A. Solid-State Redox Reactions of $LiCoO_2$ (R3m) for 4 V Secondary Lithium Cells. *J. Electrochem. Soc.* **1994**, *141*, 2972−2977.

(7) Fey, G. T. -K.; Huang, C.-F.; Muralidharan, P.; Chang, E. S. -S. Improved Electrochemical Performance of $LiCoO_2$ Surface Treated with $Li_4Ti_5O_{12}$. *J. Power Sources* **2007**, *174*, 1147−1151.

(8) Dai, X.; Wang, L.; Xu, J.; Wang, Y.; Zhou, A.; Li, J. Improved Electrochemical Performance of $LiCoO_2$ Electrodes with ZnO Coating by Radio-Frequency Magnetron Sputtering. *ACS Appl. Mater. Interfaces* **2014**, *6*, 15853−15859.

(9) Bai, Y.; Shi, H. J.; Wang, Z. X.; Chen, L. Q. Performance Improvement of $LiCoO_2$ by Molten Salt Surface Modification. *J. Power Sources* **2007**, *167*, 504−509.

(10) Park, S.-C.; Kim, Y.-M.; Kang, Y.-M.; Kim, K.-T.; Lee, P. S.; Lee, J.-Y. Improvement of the Rate Capability of $LiMn_2O_4$ by Surface Coating with $LiCoO_2$. *J. Power Sources* **2001**, *103*, 86−92.

(11) Ceder, G.; Chiang, Y.-M.; Sadoway, D. R.; Aydinol, M. K.; Jang, Y.-I.; Huang, B. Identification of Cathode Materials for Lithium Batteries Guided by First-Principles Calculations. *Nature* **1998**, *392*, 694−696.

(12) Yoon, W.-S.; Lee, K. K.; Kim, K.-B. Structural and Electrochemical Properties of $LiAl_yCo_{1-y}O_2$ Cathode for Li Rechargeable Batteries. *J. Electrochem. Soc.* **2000**, *147*, 2023−2028.

(13) Dobal, P. S.; Katiyar, R. S.; Tomar, M. S.; Hidalgo, A. Raman Spectroscopic Determination of Phase Evolutions in $LiAl_xCo_{1-x}O_2$ Battery Materials. *J. Mater. Res.* **2001**, *16*, 1−4.

(14) Cho, J.; Kim, Y. J.; Park, B. Novel $LiCoO_2$ Cathode Material with Al_2O_3 Coating for a Li ion Cell. *Chem. Mater.* **2000**, *12*, 3788−3791.

(15) Scott, I. D.; Jung, Y. S.; Cavanagh, A. S.; Yan, Y.; Dillon, A. C.; George, S. M.; Lee, S. H. Ultrathin Coatings on Nano-$LiCoO_2$ for Li-ion Vehicular Applications. *Nano Lett.* **2010**, *11*, 414−418.

(16) Chebiam, R. V.; Kannan, A. M.; Prado, F.; Manthiram, A. Comparison of the Chemical Stability of the High Energy Density Cathodes of Lithium-Ion Batteries. *Electrochem. Commun.* **2001**, *3*, 624−627.

(17) Bai, Y.; Yin, Y. F.; Liu, N.; Guo, B. K.; Shi, H. J.; Liu, J. Y.; Wang, Z. X.; Chen, L. Q. New Concept of Surface Modification to $LiCoO_2$. *J. Power Sources* **2007**, *174*, 328−334.

(18) Lee, J.-G.; Kim, T.-G.; Park, B. Metal-Phosphate Coating on $LiCoO_2$ Cathodes with High Cutoff Voltages. *Mater. Res. Bull.* **2007**, *42*, 1201−1211.

(19) Antolini, E. $LiCoO_2$: Formation, Structure, Lithium and Oxygen Nonstoichiometry, Electrochemical Behaviour and Transport Properties. *Solid State Ionics* **2004**, *170*, 159−171.

(20) Kosova, N. V.; Devyatkina, E. T. Comparative Study of $LiCoO_2$ Surface Modified with Different Oxides. *J. Power Sources* **2007**, *174*, 959−964.

(21) Chen, Z.; Dahn, J. R. Effect of a ZrO_2 Coating on the Structure and Electrochemistry of Li_xCoO_2 When Cycled to 4.5 V. *Electrochem. Solid-State Lett.* **2002**, *5*, A213−A216.

(22) Li, C.; Zhang, H. P.; Fu, L. J.; Liu, H.; Wu, Y. P.; Rahm, E.; Holze, R.; Wu, H. Q. Cathode Materials Modified by Surface Coating for Lithium Ion Batteries. *Electrochim. Acta* **2006**, *51*, 3872−3883.

(23) Zhao, H. L.; Gao, L.; Qiu, W. H.; Zhang, X. H. Improvement of Electrochemical Stability of $LiCoO_2$ Cathode by a Nano-Crystalline Coating. *J. Power Sources* **2004**, *132*, 195−200.

(24) Taguchi, N.; Akita, T.; Sakaebe, H.; Tatsumi, K.; Ogumi, Z. Characterization of the Surface of $LiCoO_2$ Particles Modified by Al and Si Oxide Using Analytical TEM. *J. Electrochem. Soc.* **2013**, *160*, A2293−A2298.

(25) Quan, Z.; Osokoshi, T.; Sonoyama, N. Synthesis and Electrochemical Property of $LiCoO_2$ Thin Film Coated on the Surface of Carbon and Anatase TiO_2 Powders. *J. Alloys Compd.* **2012**, *541*, 137−143.

(26) Fang, T.; Duh, J.-G.; Sheen, S.-R. $LiCoO_2$ Cathode Material Coated with Nano-Crystallized ZnO for Li-ion Batteries. *Thin Solid Films* **2004**, *469*, 361−365.

(27) Oh, S. W.; Myung, S.-T.; Oh, S.-M.; Yoon, C. S.; Amine, K.; Sun, Y.-K. Polyvinylpyrrolidone-Assisted Synthesis of Microscale C-$LiFePO_4$ with High Tap Density as Positive Electrode Materials for Lithium Batteries. *Electrochim. Acta* **2010**, *55*, 1193−1199.

(28) Zheng, Z.; Wang, Y. J. 3D Structure of Electrode with Inorganic Solid Electrolyte. *Electrochem. Soc.* **2012**, *159*, A1278−A1282.

(29) Noh, S.; Kim, J.; Eom, M.; Shin, D. S. Surface Modification of $LiCoO_2$ with $Li_{3x}La_{2/3-x}TiO_3$ for All-Solid-State Lithium Ion Batteries Using Li_2S-P_2S_5 Glass-Ceramic. *Ceram. Int.* **2013**, *39*, 8453−8458.

(30) Xie, J.; Imanishi, N.; Zhang, T.; Hirano, A.; Takeda, Y.; Yamamoto, O. Li-Ion Transport in All-Solid-State Lithium Batteries with $LiCoO_2$ Using NASICON-Type Glass Ceramic Electrolytes. *J. Power Sources* **2009**, *189*, 365−370.

(31) Sha, Y. J.; Yuan, T.; Zhao, B. T.; Cai, R.; Wang, H.; Shao, Z. P. Solid Lithium Electrolyte-$Li_4Ti_5O_{12}$ Composites as Anodes of Lithium-Ion Batteries Showing High-Rate Performance. *J. Power Sources* **2013**, *231*, 177−185.

(32) Vijayakumar, M.; Inaguma, Y.; Mashiko, W.; Crosnier-Lopez, M. P.; Bohnke, C. Synthesis of Fine Powders of $Li_{3x}La_{2/3-x}TiO_3$ Perovskite by a Polymerizable Precursor Method. *Chem. Mater.* **2004**, *16*, 2719−2724.

(33) Toby, B. H. EXPGUI, A Graphical User Interface for GSAS. *J. Appl. Crystallogr.* **2001**, *34*, 210−213.

(34) Reimers, J. N.; Dahn, J. R. Electrochemical and in Situ X-ray Diffraction Studies of Lithium Intercalation in Li_xCoO_2. *J. Electrochem. Soc.* **1992**, *139*, 2091−2097.

(35) Chen, N.; Yao, Y.; Wang, D.; Wei, Y.; Bie, X.; Wang, C.; Du, F. $LiFe(MoO_4)_2$ as a Novel Anode Material for Lithium-Ion Batteries. *ACS Appl. Mater. Interfaces* **2014**, *6*, 10661−10666.

DOI: 10.1021/am507421y
ACS Appl. Mater. Interfaces 2015, 7, 1787−1794